Calculated electron paramagnetic resonance *g* tensor and hyperfine parameters for zinc vacancy and N related defects in ZnO

Klichchupong Dabsamut ⬤,[1,2,*] Adisak Boonchun ⬤,[2] and Walter R. L. Lambrecht ⬤[1,†]

[1]*Department of Physics, Case Western Reserve University, 10900 Euclid Avenue, Cleveland, Ohio 44106-7079, USA*

[2]*Department of Physics, Faculty of Science, Kasetsart University, Bangkok 10900, Thailand*

Various defects in ZnO, focused on substitutional N on the O site (N_O) and N_2 at various sites—the O site, interstitial sites, and the Zn site—are studied using first-principles calculations with the goal of understanding the electron paramagnetic resonance (EPR) center reported for N_2 in ZnO and substitutional N on the O site. The *g* tensors are calculated using the gauge-including projector augmented wave (GIPAW) method and compared with experiments. The *g* tensors of the free N_2^+ and N_2^- radicals and their various contributions within the GIPAW theory are analyzed first to provide a baseline reference for the accuracy of the method and for understanding the N_2 behavior in ZnO. Previous controversies regarding the site location of N_2 in ZnO for this EPR center and regarding the shallow or deep nature and donor or acceptor nature of this center are resolved. We find that the N_2 on the Zn site is mostly zinc-vacancy-like in its spin density and *g* tensor, while for the O site, a model with the N_2 axis lying in the basal plane and the singly occupied π_g orbital along the **c** axis provides good agreement with experiment. For interstitial locations, if the N_2 is not strongly interacting with the surroundings, no levels in the gap are found and hence also no possible EPR center. The calculated *g* tensors for N_O and zinc vacancy are also found to be in good agreement with experiment. The use of different functionals affecting the localization of the spin density is shown to affect the *g*-tensor values.

I. INTRODUCTION

Electron paramagnetic resonance (EPR) provides one of the most powerful methods to study defect electronic structure. The *g* tensor, which describes the spin splitting of a defect level in a magnetic field as a function of the magnetic field magnitude and direction, provides a unique fingerprint for the defect. Along with the hyperfine tensor, which describes the interaction with nuclear spins associated with the defect, the chemical identity of a defect can readily be determined. In combination with optical or thermal excitation or quenching of the EPR center, information about the defect levels can be obtained. However, *g* tensors are rarely calculated from first principles. Defects are usually described in periodic boundary conditions, and it is only fairly recently that the methodologies for calculating *g* tensors were developed for periodic systems. These methodologies require calculating the induced current response to an external magnetic field or the orbital magnetization. This nontrivial problem was first solved for nuclear magnetic resonance (NMR) chemical shielding factors by including the gauge-induced changes in the phases of the wave function in work by Mauri and co-workers [1,2]. Subsequently, Ziegler and co-workers developed these approaches in the context of atom-centered basis sets [3,4] and Pickard and Mauri developed an implementation in terms of the projector augmented wave methods [5,6], known as the gauge-including projector augmented wave (GIPAW) method.

More recently, Ceresoli *et al.* developed a nonperturbative approach based on Berry phases [7] and also further improved the GIPAW code. The GIPAW method was applied to a number of defect systems by Gerstmann and co-workers [8–10] and Skachkov and co-workers [11–13]. These works illustrate the capability of the combination of theory and experiment in EPR to distinguish various defect models for a given EPR center.

Here we apply the GIPAW method to the study of several defects in ZnO. Our initial motivation was the work by Garces *et al.* [14] identifying N_2 in ZnO. They identified N_2 unequivocally on the basis of the characteristic hyperfine interaction with two $I = 1$ N nuclei and hypothesized that the N_2 occurred on an O site. They found an axially symmetric *g* tensor with the symmetry axis along the *c* axis of the wurtzite structure of ZnO. Subsequently, a computational study by Lambrecht and Boonchun [15] proposed instead a Zn-vacancy location for the N_2 based on the fact that the *g* tensor agrees more closely with that of a N_2^+ radical than with that of a N_2^- radical. In fact, when N_2 sits on a Zn site, it behaves as a double acceptor with the ten valence electrons of N_2 compared with the 12 valence electrons of Zn (including the filled 3*d* shell). The N_2 molecule, which then plays the role of a 2+ ion, would miss two electrons from its highest occupied molecular orbital (HOMO) σ_{g+} level. The $q = -1$ state of the defect then corresponds to the singly occupied σ_{g+} state (or a N_2^+ radical) and is EPR active. The *g* tensor of this N_2^+ radical was calculated by Bruna and Grein [16] and is characterized by a negligible $\Delta g_\parallel$ shift from the free-electron value in the direction parallel to the bond and negative $\Delta g_\perp$ in the direction perpendicular to the bond. This is readily

---
*klichchupong.d@gmail.com
†walter.lambrecht@case.edu

understood in terms of second-order perturbation theory in which the Δg tensor arises from the cross effect of spin-orbit coupling and the orbital Zeeman effect and can be written as

$$\Delta g_{ij} = 2\lambda \sum_n \frac{\langle 0|L_i|n\rangle \langle n|L_j|0\rangle}{E_0 - E_n}, \qquad (1)$$

where λ is the atomic spin-orbit coupling, $|0\rangle$ is the singly occupied molecular orbital (SOMO) whose spin splitting we try to calculate and $|n\rangle$ are the other states with energy E_0 and E_n, respectively, and L_i and L_j are the Cartesian components of the angular momentum operator. Since the angular momentum matrix elements from the SOMO σ_{g+} state can here only couple to the higher-lying π_g lowest unoccupied molecular orbital (LUMO) for the components perpendicular to the axis of the molecule, this gives a negative contribution to the $\Delta g_\perp$ as was indeed observed in the work of Garces *et al.* [14]. Lambrecht and Boonchun estimated this $\Delta g_\perp$ for the N_2 molecule, using a tight-binding model for the N_2 molecule with parameters fitted to density functional theory (DFT) calculation and using a calculated atomic spin-orbit coupling parameter, to be -2600 ppm in excellent agreement with Bruna and Grein's [16] calculation, which gave a value of -2734 ppm. Both are in good agreement with the angular average of Δg, which amounts to $\sim(2/3)\Delta g_\perp$ and experimentally is about -1900 ppm. The latter calculation was based on a more advanced quantum chemical calculation of the molecular levels but used a similar perturbation theoretical approach.

On the other hand, on an O site one would expect the N_2 molecule to behave as a donor with an additional electron in the π_g state of the molecule, which then becomes a N_2^- radical. One then would expect a positive $\Delta g_\perp$ tensor within the same type of perturbation theory, as we will show explicitly later in Sec. III A. The g tensors of N_2^- on anion sites in MgO and KCl and other ionic compounds are well known [17]. They are a bit more complex because the crystal environment breaks the degeneracy of the π_g state [17]. The main argument of Lambrecht and Boonchun [15] was that the g tensors of N_2 occurring on anion sites in these crystals differ significantly from those observed by Garces *et al.* [14]. However, in retrospect, it seems somewhat inconsistent that to explain the size of the hyperfine splitting, one needs to assume a significant delocalization of the spin density beyond the molecule while for the g tensor these models focused exclusively on the isolated molecule. Also, besides spin-orbit and orbital Zeeman perturbations, the full theory of g tensors as implemented in the GIPAW code includes additional contributions, such as the spin-other-orbit terms, which involve the magnetic field induced by the first-order induced current, diamagnetic contributions, and so on. It seems worthwhile to apply this method to reevaluate the g tensor for N_2 in ZnO.

The proposal by Lambrecht and Boonchun [15] that N_2 on Zn would be a relatively shallow acceptor was exciting because this could potentially lead to a path to the p-type doping of ZnO, which remains a challenging problem till today [18,19]. However, their proposal was challenged in several ways. Petretto and Bruneval [20] found that the N_2 in the neutral state prefers to make a bridge-type bond to two of the surrounding O atoms while the $q = -1$ state of this molecule

prefers the isolated site similar to the calculation of Lambrecht and Boonchun. However, this much lower energy of the N_2 neutral state then leads to a much deeper zero-charge-to-negative-charge transition level making the system a deep, rather than a shallow, acceptor. Furthermore, they showed that energetically, N_2 prefers the O site over the Zn site. Earlier, Nickel and Gluba [21] found several N_2 interstitial sites in ZnO to have lower energy than on the O site.

The claim of a shallow acceptor behavior of N_2 in ZnO was also challenged by an experimental study by Philipps *et al.* [22] which studied the recharging behavior of the EPR-active state. This study, like that of Garces *et al.* [14], found that upon irradiation with light, above a critical phonon energy of about 1.9 eV a new signal identified with substitutional N on the O site (N_O) becomes activated, but unlike the Garces *et al.* study it also found the N_2 signal to increase already at 1.4 eV while Garces *et al.* found irradiation to quench the EPR signal of N_2. To explain this, Philipps *et al.* proposed that their sample could be inhomogeneous with different Fermi level positions in different regions of the sample placing the Fermi level close to the defect level of the N_2, whereby not all N_2 centers would originally be in the EPR-active state. They associate the 1.4 eV activation energy with a transition from the defect to the conduction band and thus concluded that the levels were deep. While they do not explicitly discuss which site the N_2 is located on, this also suggests that the EPR-active state is in a positive charge state because it requires removing an electron from the defect to the conduction band, and hence that N_2 in ZnO is donorlike. That would, in fact, correspond to the proposal of Garces *et al.* [14]. However, alternative explanations for the recharging behavior could still be possible, and an explanation for the g tensor itself is lacking.

From the above, it is clear that several open questions remain regarding N_2 in ZnO. This makes it worthwhile to revisit the N_2 calculations at different sites, namely, O, interstitial, and Zn, and explore whether different orientations of the molecule can occur. Calculating the g factors should help to identify which of these various possible models corresponds to the experimental EPR signal, and the corresponding energy levels at the hybrid functional level can be compared with experiment. To complement this study, we also calculate the N_O g tensor. We start from first-principles calculations for both the N_2^- and N_2^+ molecules and compare these with previous calculations as a test of the accuracy of the method.

As we will show, only the N_2 on the O site originally proposed by Garces *et al.* [14] has a clear spin localization on the N_2 molecule. The other systems have spin densities mostly on surrounding O atoms or very delocalized spin density. This suggests that the N_2 on the Zn-site electronic structure is closely related to the zinc vacancy (V_{Zn}). We thus also calculate the g factor for the Zn vacancy, for which experimental data are also available. Good agreement with these experimental g-tensor data is established. For the interstitial location, in models in which the N_2 minimally perturbs the system, we find no levels in the gap and hence that the positive charge state corresponds to removing charge from the valence band maximum (VBM), leading to a very delocalized spin density and g tensors not compatible with the experimental data for N_2 in ZnO.

We will show that the N_2 on the O site can explain the data qualitatively if we assume that the experiment measures some unresolved average over different symmetry-equivalent orientations of the defect. The results are also sensitive to the density functional used as discussed in Sec. II. We also calculate the g factor for the case of substitutional N on O and find reasonable agreement assuming again that some degree of averaging occurs in the experiment. These results indicate that it might be possible to further resolve these EPR signals into separate centers corresponding to different orientations of the electronic structure on symmetry-equivalent orbitals in future work, perhaps using higher magnetic fields and microwave frequencies to improve the resolution.

II. COMPUTATIONAL METHOD

The initial defect relaxations are carried out at the hybrid functional level using a parametrized Heyd-Scuseria-Ernzerhof (HSE) potential [23] in which the fraction of exact exchange α is set to 0.375 and the inverse screening length parameter $\mu = 0.2$ Å^{-1} is used to cut off the long-range part of the exact exchange. The relaxation calculations were carried out using the Vienna *ab initio* simulation package (VASP) code [24–27] using well-converged plane-wave cutoff energy (500 eV) in the projector augmented wave (PAW) [28] method. Supercells of 128 atoms were used to model the defects.

Unfortunately, the GIPAW code has not yet implemented hybrid functionals but can, since the implementation of recent improvements, include Hubbard-U terms. It is integrated with the QUANTUM ESPRESSO (QE) code [29], which provides similar functionality to the VASP code. After determining the self-consistent potential of the system with a standard QE run, the GIPAW code evaluates the first-order induced current using density functional perturbation (DFPT) and from this extracts various g-tensor contributions, including the magnetic field induced by the first-order current from the Biot-Savart law, which leads to the spin-other-orbit contributions. It also includes other relativistic corrections besides spin-orbit coupling and distinguishes paramagnetic and diamagnetic contributions as explained in detail in Refs. [5,6]. For most of the g-tensor calculations we use the generalized gradient approximation (GGA) in the Perdew-Burke-Ernzerhof (PBE) parametrization [30] but at the atomic positions relaxed with the hybrid functional. In some cases we also used Hubbard-U corrections to the PBE functional, which can simulate the hybrid functional effects in creating an orbital-dependent potential with stronger hole localization. We checked that the hybrid functional with the parameters used here satisfies the generalized Koopmans's theorem [31–34] quite well for all of the defects considered here and at the same time provides an accurate band gap of 3.4 eV. We note that our band gap agrees well with the previous HSE calculations using $\alpha = 0.375$ and with experiment [35–37]. Details about these tests are given in the Supplemental Material [38]. We use these calculations to evaluate defect transition levels using the standard defect formation energy formalism as outlined by Freysoldt *et al.* [39] and to determine the structural models of the defects.

These same relaxed structures are then used to calculate g tensors either in PBE or in PBE + U. Adding Hubbard-U

TABLE I. Δg tensor of the N_2^+ radical in ppm: comparison with other calculations and contributions to GIPAW (PBE) as detailed in Ref. [6].

Contribution	$\Delta g_\parallel$	$\Delta g_\perp$
Total GIPAW (PBE)	−121	−3180
Total GIPAW (PBE + U)	−125	−3126
Total Bruna and Grein[a]	−249	−2734
Total tight-binding model[b]	0	−2600
Relativistic mass	−259	−259
SO bare	49	−704
SO paramagnetic	0.2	−2271
SO diamagnetic	8	12
SOO	81	42

[a]Bruna and Grein [16].
[b]Lambrecht and Boonchun [15].

terms to adjust to hybrid functional results is not trivial. One has several choices: U can be added on Zn-d, O-p, and/or N-p orbitals. Our aim is not to provide a fully optimized choice but to gain insight into the qualitative effects of adding specific U terms.

Hyperfine tensors were also calculated using the GIPAW code. They make use of the PAW reconstruction of the full atomic wave function including relativistic corrections [40–42].

III. RESULTS

A. N_2 radicals

1. g tensors

We start with the results for the g tensors of the N_2 molecule in the +1 and −1 charge states as shown in Tables I and II. We can see from these tables that the dominant contributions to $\Delta g_\perp$ are the spin-orbit (SO) paramagnetic and bare terms. The bare term refers to the pseudo part of the wave function, and the paramagnetic term corresponds to the PAW-reconstructed parts of the full atomic wave function. The diamagnetic and spin-other-orbit (SOO) contributions are small. The agreement with other calculations which use a much simpler approach is excellent. The Bruna and Grein approach [16] calculates first-order contributions to Δg at the realistic open-shell Hartree-Fock level, and the second-order terms correspond to the cross terms of orbital Zeeman and spin-orbit coupling, essentially as in Eq. (1). In the GIPAW

TABLE II. Calculated Δg (in ppm) terms for N_2^- using the GIPAW approach.

Contribution	$\Delta g_\parallel$	$\Delta g_\perp$
Total GIPAW	53	1741
Relativistic mass	−2	−2
SO bare	14	447
SO paramagnetic	41	1296
SO diamagnetic	0.1	0.1
SOO	−0.2	−0.4

TABLE III. Hyperfine tensor parameters for N_2^+ and N_2^- in megahertz.

	A_{dip}	A_{iso}
	N_2^+	
This paper, PBE	-30.4	102.2
This paper, PBE $+ U$	-29.9	95.6
Experimental	23.3[a]	102.4[a]
		104.1[b]
Other calculated	29.7[c]	91.3[c]
	N_2^-	
This paper, PBE	-0.14	2.92
This paper, PBE $+ U$	-0.13	2.99

[a]Scholl *et al.* [43].
[b]Knight *et al.* [44].
[c]Bruna and Grein [16].

approach the relativistic mass term and diamagnetic terms are also first-order terms in the sense that they are calculated from expectation values using the zeroth-order wave functions. The SOO and SO paramagnetic and bare terms are second-order corrections to the energy since they involve first-order wave functions. Thus the sum of SO diamagnetic and relativistic mass corrections should be compared with the Bruna and Grein value for $\Delta g_\parallel$. The orientation-averaged Δg in our present GIPAW calculation is -2160 ppm, which is close to the experimental value of -1900 as reported by Bruna and Grein [16]. The above values were obtained in PBE. When adding a U on N-p orbitals of 3 eV, the values change slightly. We only report the decomposition in partial contributions for the PBE case. The decomposition is similar, with the SO diamagnetic mass corrections and SOO almost unchanged and the differences arising mostly from the SO paramagnetic and bare terms, which indeed depend on energy level splittings because they are second-order corrections to the energy. This calculation provides a good benchmark for the accuracy of the GIPAW approach. For the N_2^- radical we find again that the dominant contributions are the paramagnetic and bare SO terms. They are positive in this case, and this is easy to understand from Eq. (1) since now the unpaired spin is in the π_g state and it can give nonzero off-diagonal matrix elements of the angular momentum operator with two lower-lying σ_g states. In this calculation, we have occupied one of the degenerate π_g states and thereby broken the symmetry in our spin-polarized DFT calculation. This confirms that the N_2^+ and N_2^- radicals have opposite signs of the main $\Delta g_\perp$. Of course these results correspond to the isolated molecule, and this may change when the molecule is placed in a crystal environment and other levels of the system become involved.

2. Hyperfine tensors

The hyperfine tensor for the diatomic molecule contains a dipole part which is axial with parameters $A_\perp = A_{\mathrm{dip}}$, $A_\parallel = -2A_\perp$ and the isotropic Fermi contact term A_{iso}. Our calculated values compared with experiment and other calculations are given in Table III. Note that the experiment does not detect the sign of the hyperfine tensor. The agreement is quite good.

The Fermi contact term depends slightly on the functional. Interestingly, while adding U is expected to make the wave function more localized, its Fermi contact term nonetheless slightly decreases. This must indicate that the s component of the wave function is slightly decreased. Note that we included U on the N-2p orbital. Various other calculated results are reviewed by Bruna and Grein [16] and give a range of values with average 88 ± 10 for the Fermi contact term. For the N_2^- radical, we find a much smaller hyperfine interaction. For the isotropic Fermi contact term, this is clearly related to the fact that the unpaired spin in this case is in a π_g state and has no direct s contribution to the wave function.

B. Zn vacancy

1. g tensors

Next we consider the Zn vacancy. Unconstrained relaxations carried out in the hybrid functional led to a model in which the spin is clearly localized on a single O atom which moved away from the vacancy, thus forming a polaronic state. This can be seen in Fig. 1. In this case, it was localized on a lateral O atom in the basal plane next to the vacancy, and thus the system has only C_s symmetry, containing only a mirror plane. The **a**, **b**, and **c** vectors in this figure are the lattice vectors of the supercell and correspond to the $[01\bar{1}0]$, $[\bar{2}110]$, and $[0001]$ directions. Thus the spin density is seen to lie in a $(\bar{2}110)$ plane and with the smallest $(\Delta g < 0)$ principal axis closer to the **c** axis. On the other hand, if the spin localizes on the axial O atom, the symmetry of the system remains C_{3v}. Experimentally, both of these cases have been observed in the work of Galland and Herve [45], and the V_{Zn} EPR center was also studied by Son *et al.* [46], who identified a separate center with H attached to the O atom in the V_{Zn}. Here, we only discuss the V_{Zn}. The g tensor and its principal axes are given in Table IV.

We can see that in the experiment, the smallest g component is still larger than the free-electron value $g_e = 2.002\,319$ and has its principal axis at $69.25°$ from the **c** axis in a $\langle 1\bar{2}10 \rangle$ plane, which is a mirror plane of the wurtzite structure. Note that the opposite direction is $111°$ from the **c** axis, which is close to the $109°$ ideal tetrahedral angle, which means that this direction is the direction of the broken Zn-O bond. Thus, as usual, the lowest Δg that occurs is along the direction of the dangling bond. The two other principal values are close to each other and are larger and positive. This is also consistent with the C_{3v} center with the hole localized on the axial O atom, in which case the experimental values are $g_\parallel = 2.0024$ and $g_\perp = 2.0193$. Comparing with the PBE-calculated values, we see that the g tensor still lies in a $\langle 1\bar{2}10 \rangle$ plane but the smallest value is now negative and at $38°$ or $142°$ from the **c** axis. Adding a Hubbard-U term of 5 eV on the O-p orbitals makes this Δg positive but overshoots slightly compared with experiment. The angle θ_c from the **c** axis is now $73°$, or $107°$, much closer to the experiment and to the dangling bond direction. The wave function also becomes more localized exclusively on this one O atom [as shown in Fig. 1(b)], while in PBE it had some small components on the other two lateral O neighbors of the Zn vacancy. This is as expected from DFT $+ U$, in which the U term tends to make the spin density more localized by pushing the hole state deeper into the gap.
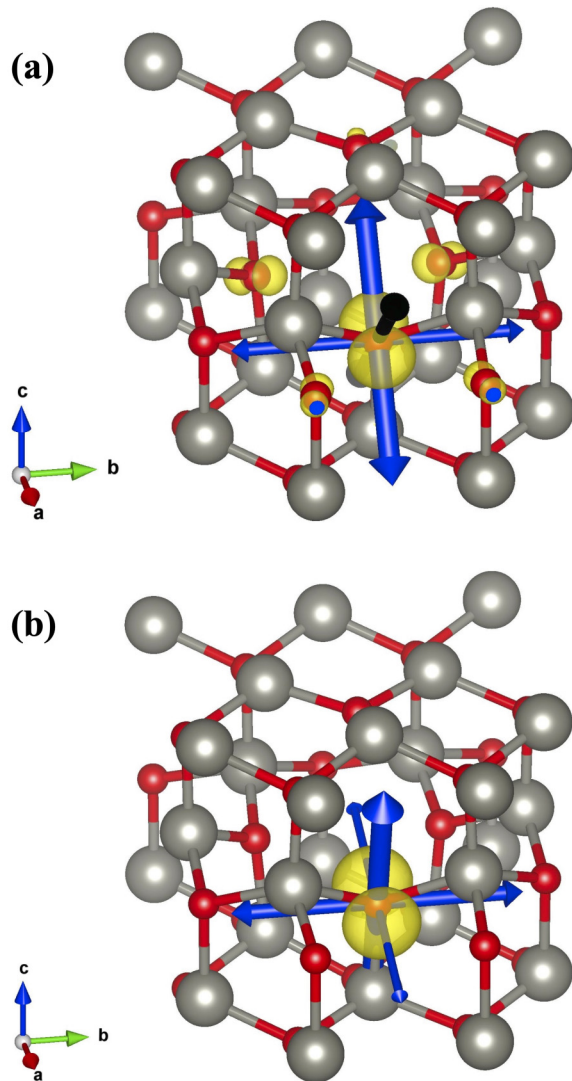
FIG. 1. Relaxed structure in (a) PBE and (b) PBE $+ U$ near the V_{Zn} in the EPR-active $q = -1$ charge state, showing the net spin density as a yellow isosurface. The double-sided vectors show the Δg tensor principal axes, and the thickness of the vectors indicates how big the magnitude of $|\Delta g|$ is; black and blue represent negative and positive values, respectively.

TABLE IV. The g tensor and principal axes for the V_{Zn}.

	g_1	g_2	g_3
Experimental[a]	2.0028	2.0173	2.0183
Principal axes	$\theta_c = 69.25°$	$\theta_c = 20.75°$	
	in $\langle 1\bar{2}10 \rangle$		$\perp \langle 1\bar{2}10 \rangle$
Calculated PBE	1.9948	2.0166	2.0096
Principal axes	$\theta_c = 38°$	$\theta_c = 52°$	
	in $\langle 1\bar{2}10 \rangle$		$\perp \langle 1\bar{2}10 \rangle$
Calculated PBE $+ U$	2.0039	2.0095	2.0092
Principal axes	$\theta_c = 73°$	$\theta_c = 17°$	
	in $\langle 1\bar{2}10 \rangle$		$\perp \langle 1\bar{2}10 \rangle$

[a]Galland and Herve [45].

These results confirm the basic model proposed by Galland and Herve [45], who analyzed the Δg tensor essentially based on Eq. (1) and viewed it as originating from the splitting between the O-p state on which the hole is localized and the O-p state in its perpendicular directions. Since the hole is a localized O-p-type dangling bond, it lies above the other O-p states, and the SO contribution to Δg is thus positive for $g_\perp$ and negligible for $g_\parallel$ in their model. The full calculation indicates that the $\Delta g_\parallel$ is not exactly zero and is also slightly positive. The details depend obviously sensitively on the degree of localization of the wave function. All the models considered here including U give better results than the pure PBE results because the latter have a wave function too delocalized on other nearby O atoms next to the vacancy even though we already created some difference between the three lateral O atoms by relaxing the structure within the hybrid functional.

Our HSE and PBE $+ U$ calculations show that the defect transition levels for V_{Zn} are 1.38 and 0.29 eV, respectively. The HSE result agrees with the result from previous studies of 1.4 eV [47,48]. The PBE $+ U$ gives a significantly less deep level, consistent with previous research which gives values in the range 0.17–0.3 eV [37,49,50].

2. Hyperfine parameters

For the V_{Zn} the spin localizes on a single oxygen atom. Oxygen has only isotope ^{17}O with nonzero nuclear spin $I = 5/2$, and this isotope has only 0.038% natural abundance. Nonetheless, calculating it gives a value of $A_{dip} = 74$ MHz and $A_{iso} = 27$ MHz on the oxygen atom on which the spin is localized.

For Zn there is one isotope ^{67}Zn with spin $I = 5/2$ which has 4.10% abundance. We find non-negligible Fermi contact terms hyperfine on only three of the Zn atoms in the cell, namely, the three that are nearest neighbors to the oxygen atom on which the spin is localized. Their hyperfine tensors A_{iso} range from -13.7 to -16.7 MHz. The dipolar parts $A_{dip} \approx 1$ MHz.

C. Substitutional N on the O site

Next, we turn our attention to the substitutional N_O case. This is a well-studied defect and found to have a very deep zero-charge-to-negative-charge transition level. The
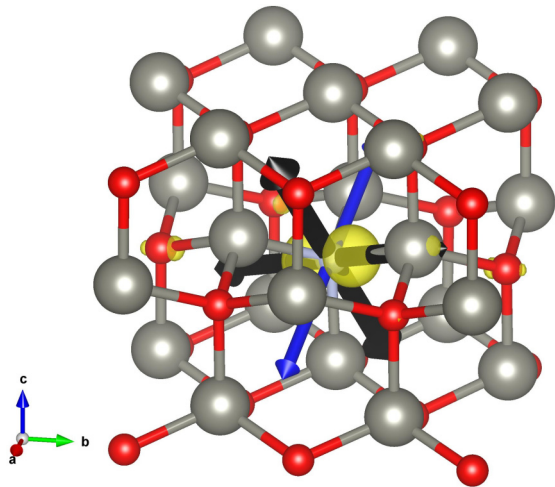
The principal values in the directions perpendicular to the dangling bond are smaller than in experiment but indeed larger than along the dangling bond and closer to each other than in the PBE case. Using a smaller value of $U = 3$ eV gives $g_1 = 2.0054$, $g_2 = 2.0117$, and $g_3 = 2.0128$, giving a larger overestimate of the small g_1 (which we might call $g_\parallel$, "$\parallel$" meaning parallel to the dangling bond) and larger values for g_2 and g_3 (which we might average to $g_\perp$), which are closer to experiment. Further inspection of the Δg contributions shows that the SOO contribution is small and increasing U increased the paramagnetic SO contribution for both parallel and perpendicular directions. Adding a $U_d = 6$ eV on the Zn-d orbital and $U_p = 3$ eV on the O-p orbital reduced $g_\parallel$ to 2.0036 but also reduced $g_\perp$ to 2.0097. The directions of the principal axes barely changed.

FIG. 2. Spin density for N_O in the neutral charge state and EPR g factor.

result from our HSE calculation of 2.02 eV is a bit deeper than previously obtained values [15,51]. However, our PBE $+ U$ functional gives a value of 0.56 eV, while a study using the local-density approximation (LDA) in its calculations reported a value of 0.4 eV [52]. The spin density of the neutral charge state is shown in Fig. 2. The g tensor is compared with experiment in Table V. The unconstrained relaxation gave a spin density localized mostly on N on a p orbital approximately along the b direction ($[\bar{2}110]$) and with small contributions on various second-neighbor O atoms, as can be seen in Fig. 2. In the experiment the $g_\parallel$ corresponds to the $\mathbf{c}$ axis and is fully axially symmetric, while we find a higher anisotropy. At first, one might assume that this just means that the spin became localized on a N-p_z orbital along the $\mathbf{c}$ axis in the experiment. However, we may also assume that the experiment sees an average of centers with spin localized in the basal plane and along $\mathbf{c}$. Also, our value of $\Delta g_\parallel = 6981$ ppm is positive, while the experimental value is negative. For our calculations, "$g_\parallel$" indicates the g tensor-component parallel to the unpaired spin orbital, "$g_\perp$" indicates the g tensor-component in the basal plane perpendicular to the spin orbital, and "g_c" indicates the g tensor-component along the $\mathbf{c}$ axis. Averaging the values in the $\mathbf{c}$ direction, assuming three orientations that are equivalent in the basal plane and one that is along the $\mathbf{c}$ axis, we can write $\bar{g}_c = (g_\parallel + 3g_c)/4$, which gives a value of 1.988. For the direction perpendicular to $\mathbf{c}$ we can write $\bar{g}_{\perp c} = [(g_\parallel + g_\perp)3/2 + (g_c + g_\perp)/2]/4 = 1.993$. This gives two negative Δg values close to each other as in the experi-

TABLE V. The g tensors for N_O.

	$g_{\parallel c}$	$g_{\perp c}$	
Experimental[a]	1.995	1.963	
	$g_\parallel$	g_c	$g_\perp$
PBE	2.0093	1.9810	1.9843
Principal axes	$\theta_b = 27°$	$\theta_c = 36°$	$\theta_a = 36°$
PBE $+ U_{\text{N-}p} = 3$ eV	2.0062	2.0014	2.0029

[a]Philipps *et al.* [22].

ment but fails to capture the small difference between the g tensor in the basal plane and the g tensor along $\mathbf{c}$ observed in the experiment. There might be some energetic advantage to the spin localizing in the $\mathbf{c}$ direction which would then explain the smaller negative value in the $\mathbf{c}$ direction. Adding U values of 3 or 5 eV on N or on both N and O did not change the orientation of the spin density or its degree of localization. It tends to make the Δg values closer to each other and smaller, but no improvement in relation to the experimental values was obtained.

It was found experimentally [22] that the N_O center is activated by light with photon energy of about 1.9 eV. We have thus calculated the energy of the vertical transition from the negative charge state to the neutral one plus an electron at the conduction band minimum (CBM). Including only the image charge correction to the negative charge state, we obtain 1.98 eV for this activation. However, recently, it was proposed [53] that even the neutral charge state in the frozen geometry of the negative charge state requires a correction due to the presence of polarization charge and this needs to be screened using only the electronic screening. This gives a value of 2.25 eV. Both values are in reasonable agreement with the experiment.

As for the hyperfine tensor for N_O, we find $A_{\text{iso}} = 24$ MHz and $A_{\text{dip}} = -27$ MHz on the N atom with the $A_\parallel = -2A_{\text{dip}}$ along the $\mathbf{c}$ axis. Thus we obtain $A_{\parallel c} \approx 78$ and $|A_{\perp c}| \approx 3$ MHz. Philipps *et al.* [22] give values of $A_{\parallel c} = 81$ and $A_{\perp c} = 8.5$ MHz. These values are in fair agreement.

D. N_2 in ZnO

1. Zn site

First we considered various models for N_2 placed inside the Zn vacancy. One of our goals here is to revisit the question of whether the N_2 at this site is a shallow or deep acceptor. We start from different initial orientations of the molecule, either parallel to $\mathbf{c}$ or in the basal plane and in the basal plane either with the molecular axis pointing toward one of the neighboring O atoms or with the molecular axis pointing perpendicular to it. We also started either from the ideal crystal or from the previously relaxed vacancy. To summarize these results, we found that the lowest energy for the neutral charge state has the N_2 forming a bridgelike bond along one of the tetrahedral sides surrounding the vacancy and connecting to two O atoms. This configuration, also reported by Petretto and Bruneval [20], has about 0.465 eV lower energy than the in-basal-plane configuration with the molecule aligned with one of the bonds, in which case it can still make a single N-O bond if we place it close to an O atom or can be essentially isolated. The vertically aligned molecule tended to flip back to a horizontal position or at least tilt slightly. We also shifted the center of gravity of this molecule up or down from the V_{Zn} center to keep it more isolated. On the other hand, in the EPR-active $q = -1$ charge state the isolated N_2 molecule had the lowest energy. The transition level (from zero to negative charge) is in principle calculated from the lowest energy configuration of each charge state and is then found to be 2.46 eV using the HSE functional, which is considerably deeper above the valence band maximum than the shallow one of 0.17 eV obtained using PBE $+ U$. These results support
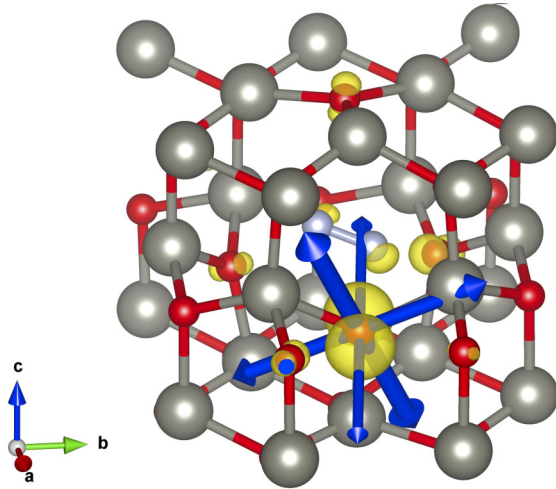
FIG. 3. N_2 in V_{Zn} relaxed structure in the $q = -1$ state with spin isosurface and g tensor.

the conclusion of Petretto and Bruneval [20] and contradict those of Lambrecht and Boonchun [15], who only considered a more isolated configuration of N_2 and furthermore proposed that the generalized Koopmans's condition is better satisfied within PBE than within PBE $+ U$ and thereby obtained a shallower defect level. Thus our first conclusion here is that N_2 on the Zn site would be a deep acceptor. Figures showing these structural models can be found in the Supplemental Material [38].

Turning now to the spin densities, we find that the spin density showed very little contribution on the N_2, mostly on a single O neighbor. This is shown in Fig. 3. The g tensor is then similar to the V_{Zn} case with all positive Δg values. Again, if the spin is oriented, for example, along the **a** direction, then the lowest Δg principal value occurs along that direction. The Δg shifts are similar to that of the vacancy. These are very different from the values reported for N_2 in ZnO by Garces *et al.* [14] and Philipps *et al.* [22], and we thus conclude that N_2 on a Zn site is incompatible with the observed EPR center. Furthermore, it implies that if N_2 were isolated in a Zn vacancy, it would only slightly perturb the vacancy and would lead to a polaronic system with spin localized on a single O atom as in the vacancy case.

2. Interstitial sites

Next we consider various interstitial sites. Among these, the lowest energy is obtained for the structure where N_2 occurs in the middle of the large hexagonal interstitial site. We constrained this model so as to allow the molecule only to move along the z direction. It is shown in the Supplemental Material [38]. In this case, we found that the N_2 molecular states are deep enough that the HOMO σ_{g+} state stays occupied and the π_g is empty. The neutral charge state shows no levels in the gap at all. Attempting to make a $q = +1$ charge state then leads to removing an electron from the VBM resulting in a very delocalized spin density. The g tensor calculated shows very large negative values along the **c** direction, about $g_c = 1.7132$, and a value of about $g_{\perp c} \approx 1.99$. We think these may reflect the g tensor of the VBM, but additional work

is needed to understand these values. The g tensors of such delocalized states as the VBM or CBM are usually discussed in terms of $\mathbf{k} \cdot \mathbf{p}$ theory [54]. We do not discuss it further here but rule out any of these sites as responsible for the observed N_2 EPR center in ZnO. Although this does not refute that N_2 could occur interstitially as claimed by Nickel and Gluba [21], it presumably has no EPR-active state in this case because no defect levels are found in the gap from which a singly occupied unpaired spin state could be constructed. Other interstitial forms of N_2 may disrupt the ZnO network and hence lead to O dangling-bond-type states as reported by Nickel and Gluba [21], but they do not lead to an EPR center with spin density on the N_2 molecule compatible with the one observed [14] and are thus not further pursued here.

3. O site

Finally, we return to the N_2 molecule at the O site as initially proposed by Garces *et al.* [14]. We started out from an initial orientation of the molecular N_2 bond axis parallel to the **c** axis. The N_2 molecule was allowed to move only in the **c** direction. After relaxation the spin density was strongly localized on the N_2 molecule and shows clearly a π_g-like state which happens to be oriented with the **a** axis. This is shown in Fig. 4(a). The defect in this case is a donor, and the spin density corresponds to the $q = +1$ charge state of the defect, which is, however, N_2^- from the view of the N_2 molecule. The defect transition level (from positive to zero charge) for this case is 3.07 using HSE (1.46 eV in PBE $+ U$). We also investigate the N_2 molecule with its bond axis perpendicular to the **c** axis. We start the configuration by pointing the N_2 toward one of neighboring Zn atoms as can be seen in the Supplemental Material [38]. After the relaxation by fixing the molecule's movement in the z direction, the N_2 molecule is pointing to the space between two Zn atoms. As in the previous model, the spin density was strongly localized on the N_2. The defect transition levels of this model, 3.23 and 1.59 eV using HSE and PBE $+ U$, respectively, are somewhat deeper than those of N_2 parallel to the **c** axis. Full unconstrained relaxation of the N_2 molecule led to an orientation intermediate between these two cases.

The g tensor for the N_2 molecule parallel to the **c** axis is found to have the lowest principal value along the direction of the N_2 axis and in fact has a negative Δg in this direction. The next-higher g-principal value is in the direction of the π_g SOMO, and the highest value is along the direction perpendicular to the plane of the molecular axis and the π orbital. This corresponds to the first and second rows in Table VI (i.e., for $N_2 \parallel \mathbf{c}$). We can see in the third and fourth rows of the table (i.e., for $N_2 \perp \mathbf{c}$, PBE and PBE $+ U$) that this is true also when the N_2 axis is fixed to be perpendicular to **c**. In case of a full relaxation, we find some intermediate orientation. We do not find convincingly lower energy among any of these orientations, which in the end result in energies within the error bar from each other.

All values slightly increase if we add a Hubbard U on both N and O, and this makes the two higher values correspond to a small positive Δg for the first case where N_2 is parallel to the **c** axis. When we fix N_2 to lie in the **c** plane, we already obtain two positive and one negative Δg in PBE; however,
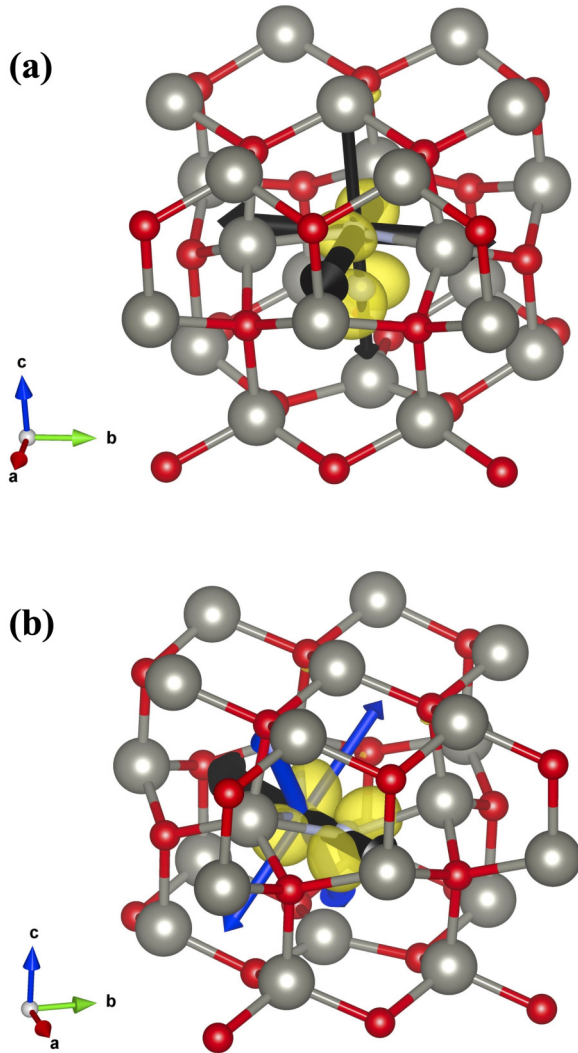
FIG. 4. Spin density and relaxed structure for N_2 at the O site with the molecular axis fixed (a) parallel and (b) perpendicular to the **c** axis.

TABLE VI. The g tensors for N_2 on the O site.

		$g_{\parallel N_2}$	$g_{\parallel \pi \text{ orb.}}$	$g_{\perp \pi \text{ orb.}}$
$N_2 \parallel \mathbf{c}$	PBE	1.95378	1.98724	2.00007
	PBE $+ U$[a]	1.98736	2.00381	2.00988
$N_2 \perp \mathbf{c}$	PBE	1.98494	2.00506	2.00911
	PBE $+ U$	1.99281	2.00457	2.00666
		$g_{\parallel c}$	$g_{\perp c}$	
	Experimental	2.0036	1.9935	
$N_2 \perp \mathbf{c}$	SOMO $\parallel \mathbf{c}$	2.0038	1.9986[b]	

[a]$U = 3$ eV on N and O.
[b]Average of the $g_{\parallel N_2}$ and $g_{\perp \pi \text{ orb.}}$ values for $N_2 \parallel \mathbf{c}$, PBE $+ U$ (i.e., the first and third values in the second row of data).

perpendicular to it, or somewhere in between. We obtain the following averages based on the g tensors in the second row of Table VI (i.e., for $N_2 \parallel \mathbf{c}$, PBE $+ U$): for the N_2 axis parallel to **c**, $g_{\parallel c} = 1.98736$ and $g_{\perp c} = 2.0068$; for the N_2 axis in the basal plane and the π orbital along **c**, $g_{\parallel c} = 2.00381$ and $g_{\perp c} = 1.9986$; and finally, for the N_2 axis in the basal plane and the π orbital perpendicular to **c**, $g_{\parallel c} = 2.00988$ and $g_{\perp c} = 1.99558$. The first choice disagrees with experiment, but both cases with the axis in the basal plane are compatible with the experimental value with a slightly better agreement if the π orbital is along the **c** axis. In fact, in this case the agreement is pretty close. Furthermore, also in the two cases (the third and fourth rows of the table, i.e., for $N_2 \perp \mathbf{c}$, PBE and PBE $+ U$) where we explicitly constrained the molecular axis to be in the plane but found the SOMO to be tilted away from the plane, we find a negative Δg perpendicular to the plane along the molecular axis, and we find that the other two directions have positive Δg with the largest one in the direction perpendicular to the plane of the molecular axis and the SOMO. This direction is found to be closest to the **c** direction, about $30°$ away from it. We may deduce from this that the experimental data are compatible with a preferred orientation of the molecular axis in or close to the basal plane. The axial symmetry along **c** observed experimentally does not correspond to a simple orientation of the molecule along this axis but rather some average over various in-plane orientations of the molecule.

The activation energy of the EPR center of $(N_2)_O$ corresponds to a transition from the neutral to the positive state releasing an electron to the conduction band minimum. This vertical transition is calculated to be 1.57 eV for the case of the molecular axis being in plane and 1.72 eV for the vertically aligned molecular axis, following the approach of Falletta *et al.* [53] for the correction terms, in other words, using here only electronic screening. These values are in reasonable agreement with the experimental observation that the EPR signal of the N_2 in ZnO is enhanced by light with photon energy as low as 1.4 eV, so somewhat lower by about 0.5 eV than the N_O substitutional defect. Since we here found the calculated N_O to have an activation energy of around 2.2 eV, this is qualitatively also in agreement with experiment.

Finally, we consider the hyperfine tensor for the N_2 on the O site. In Table VII we give the eigenvalues of the hyperfine dipolar tensor as three values in parentheses for each of the N atoms. For the $N_2 \parallel \mathbf{c}$ case, the values on both atoms differ

the SOMO is not lying in the plane but is slightly tilted as shown in Fig. 4(b). There are thus small variations in these g tensors with the functional and depending on the orientation of the molecule, but the basic correlation between molecular axes and the broken symmetry of the π_g orbital in which the hole resides stay consistent. Further inspection shows that, as usual, the mass correction, diamagnetic, and SOO contributions are small. The main paramagnetic contribution is strongly negative in both the GIPAW and bare terms for the **c** direction, while the paramagnetic GIPAW term is positive for the directions in the plane of the molecular axis and its spin orbital.

The g tensor at first does not seem to agree with the experiment, which has $g_{\parallel c} = 2.0036$ and $g_{\perp c} = 1.9935$. However, let us now consider that the molecule might be oriented in various equivalent ways and that the experiment sees an unresolved average of these. We then have several possibilities: The molecular axis might be along **c** as in the first two rows of Table VI (i.e., for $N_2 \parallel \mathbf{c}$) or perpendicular to it (third and fourth rows) with either the π orbital along **c** or the π orbital

TABLE VII. Hyperfine parameters (in megahertz) on N for N_2 on the O site.

	Atom	A_{dip}	A_{iso}
$N_2 \parallel$ **c** PBE	N_1	$(-28.5, -30.7, 59.2)$	15.7
	N_2	$(-17.0, -19.9, 36.9)$	6.3
$N_2 \perp$ **c** PBE	N_1	$(-23.1, -23.6, 46.7)$	14.6
	N_2	$(-23.4, -23.9, 47.3)$	14.9

somewhat, but their average value is still close to -23 MHz, which is also close to that of the isolated N_2^+ molecule. For the isotropic part, the value is about ten times smaller than for the N_2^+ case. This could at first sight indicate significant delocalization of the defect wave function. However, what really matters for the Fermi contact term is the contribution of the N-s state to the defect wave function. In fact, the values are significantly larger than those of the N_2^- isolated radical. The wave function here is clearly not purely p-like on N even though it is related to a π_g state. The N-p-like part of the wave function is responsible for the dipolar part, and the closeness to the values for the N_2^+ molecule indicates that the wave function is still strongly localized on the N_2.

Comparing our results with experimental data by Garces *et al.* [14] and Philipps *et al.* [22], who give $A_{\parallel c} = 9.8$ and $A_{\perp c} = 20.1$ MHz, we note that our values are $A_{\parallel N_2} = -8$ and $A_{\perp N_2} = 62$ MHz. So, if the molecule lies in the plane, $|A_{\parallel c}| = 8$ MHz, and $|A_{\perp c}|$ is the average of these two, or 27 MHz. These results are consistent with the experimental values.

4. Summary

We thus conclude that among the various models for N_2 in ZnO, only the O site gives possibly a g tensor compatible with the experiment because it is the only model with spin density localized on the N_2 molecule. In order to obtain agreement we need to assume that the N_2 molecule tends to lie preferentially with its axis in the basal plane and most likely with the π orbital containing the unpaired spin pointing in the **c** direction or close to it. In fact, there are three possible high-symmetry orientations in the plane with the molecular axis in a mirror plane vs only one along **c** for the N_2 axis, so simply statistically, it is more likely to find planar orientation. We did not find a clear energy advantage for this orientation. They were all close and also close to the fully relaxed minimum energy orientation, which was intermediate. Thus we assume that the experiment samples some average over these different orientations of the molecule. The degeneracy of the π_g state is broken with one particular orientation of the orbitals containing the unpaired spin. Because the g tensor in the direction of the bond is strongly negative, the dominant in-plane orientation of the molecular axis leads to an average negative $\Delta g_{\perp c}$ value in agreement with experiment. The otherwise mostly positive Δg values are compatible with our initial calculation for the N_2^- radical, and the largest positive value occurs for the direction

perpendicular to the plane of the SOMO, which we found to be close to the **c** axis, thus explaining the positive $\Delta g_{\parallel c}$ in the experiment. The negative value along the bond must arise somehow from the interplay with the crystal levels rather than from the molecule itself.

IV. CONCLUSIONS

In conclusion, we have carried out g-tensor calculations for isolated molecules of N_2 radicals with one electron subtracted or added and have analyzed the different contributions to it in the GIPAW theory and compared them with previous perturbation theory approaches. We have shown that the EPR signal of N_2 in ZnO is only compatible with calculated g tensors for the O site. In that case, the N_2 behaves as a deep donor, and this is compatible with the recharging studies of Philipps *et al.* [22]. For the Zn site, the N_2 molecule tends to bind to two O atoms in the neutral state but stays in an isolated nonbonding configuration in the unpaired spin-negative state. The system is then unfortunately a deep acceptor. This agrees with Petretto and Bruneval's study [20]. The spin density in this case is rather similar to that of the Zn vacancy, for which we found good agreement for the g tensor with early experimental data given by Galland and Herve [45] characterized by a positive $\Delta g_{\perp}$ tensor, where "$\perp$" means perpendicular to the dangling bond. For the interstitial sites, no levels in the gap are obtained, and hence no spin density is observed unless we remove an electron from the VBM, which gives a very different g tensor. For the simple substitutional N_O we also found a g tensor in reasonable agreement with experiment assuming that the experiment sees an average over different possible orientations of the N-p orbital on which the spin is localized. These results suggest that further experimental work on these EPR centers, possibly with higher microwave frequency and magnetic field, could help to resolve the individual centers with different orientations of the spin density.

Good agreement with experiment is also obtained for the hyperfine parameters both in the isolated molecules and for the N_2 molecule on the O site and the N_O substitutional case. We also provided hyperfine parameters for the V_{Zn}, where we find notable hyperfine parameters only on the three nearest-neighbor Zn atoms to the O atom on which the electron spin is localized.

[1] F. Mauri and S. G. Louie, Magnetic Susceptibility of Insulators from First Principles, Phys. Rev. Lett. **76**, 4246 (1996).

[2] F. Mauri, B. G. Pfrommer, and S. G. Louie, *Ab initio* NMR Chemical Shift of Diamond, Chemical-Vapor-Deposited Diamond, and Amorphous Carbon, Phys. Rev. Lett. **79**, 2340 (1997).

[3] D. Skachkov, M. Krykunov, E. Kadantsev, and T. Ziegler, The calculation of NMR chemical shifts in periodic systems based

on gauge including atomic orbitals and density functional theory, J. Chem. Theory Comput. **6**, 1650 (2010).

[4] E. S. Kadantsev and T. Ziegler, Implementation of a DFT-based method for the calculation of the Zeeman *g*-tensor in periodic systems with the use of numerical and Slater-type atomic orbitals, J. Phys. Chem. A **113**, 1327 (2009).

[5] C. J. Pickard and F. Mauri, All-electron magnetic response with pseudopotentials: NMR chemical shifts, Phys. Rev. B **63**, 245101 (2001).

[6] C. J. Pickard and F. Mauri, First-Principles Theory of the EPR *g* Tensor in Solids: Defects in Quartz, Phys. Rev. Lett. **88**, 086403 (2002).

[7] D. Ceresoli, U. Gerstmann, A. P. Seitsonen, and F. Mauri, First-principles theory of orbital magnetization, Phys. Rev. B **81**, 060409(R) (2010).

[8] E. Rauls, E. N. Kalabukhova, S. Greulich-Weber, U. Gerstmann, D. Savchenko, A. Pöppl, and F. Mauri, Nitrogen donor aggregation in 4H-SiC: g-tensor calculations, in *Silicon Carbide and Related Materials 2006*, Materials Science Forum Vol. 556 (Trans Tech, Bäch, Switzerland, 2007), pp. 391–394.

[9] U. Gerstmann, M. Rohrmüller, F. Mauri, and W. Schmidt, *Ab initio g*-tensor calculation for paramagnetic surface states: hydrogen adsorption at Si surfaces, Phys. Status Solidi C **7**, 157 (2010).

[10] G. Pfanner, C. Freysoldt, J. Neugebauer, and U. Gerstmann, *Ab initio* EPR parameters for dangling-bond defect complexes in silicon: Effect of Jahn-Teller distortion, Phys. Rev. B **85**, 195202 (2012).

[11] D. Skachkov, W. R. L. Lambrecht, H. J. von Bardeleben, U. Gerstmann, Q. D. Ho, and P. Deák, Computational identification of Ga-vacancy related electron paramagnetic resonance centers in β-Ga$_2$O$_3$, J. Appl. Phys. **125**, 185701 (2019).

[12] D. Skachkov and W. R. L. Lambrecht, Computational study of electron paramagnetic resonance parameters for Mg and Zn impurities in β-Ga$_2$O$_3$, Appl. Phys. Lett. **114**, 202102 (2019).

[13] D. Skachkov, W. R. L. Lambrecht, K. Dabsamut, and A. Boonchun, Computational study of electron paramagnetic resonance spectra for Li and Ga vacancies in LiGaO$_2$, J. Phys. D: Appl. Phys. **53**, 17LT01 (2020).

[14] N. Y. Garces, L. Wang, N. C. Giles, L. E. Halliburton, G. Cantwell, and D. B. Eason, Molecular nitrogen (N$_2$-) acceptors and isolated nitrogen (N-) acceptors in ZnO crystals, J. Appl. Phys. **94**, 519 (2003).

[15] W. R. L. Lambrecht and A. Boonchun, Identification of a N-related shallow acceptor and electron paramagnetic resonance center in ZnO: N$_2^+$ on the Zn site, Phys. Rev. B **87**, 195207 (2013).

[16] P. J. Bruna and F. Grein, The A$^2\Pi_u$ state of N$_2^+$: Electric properties, fine and hyperfine coupling constants, and magnetic moments (*g*-factors). A theoretical study, J. Mol. Spectrosc. **250**, 75 (2008).

[17] F. Napoli, M. Chiesa, E. Giamello, M. Fittipaldi, C. Di Valentin, F. Gallino, and G. Pacchioni, N$_2^-$ radical anions trapped in bulk polycrystalline MgO, J. Phys. Chem. C **114**, 5187 (2010).

[18] J. G. Reynolds, C. L. Reynolds, A. Mohanta, J. F. Muth, J. E. Rowe, H. O. Everitt, and D. E. Aspnes, Shallow acceptor complexes in p-type ZnO, Appl. Phys. Lett. **102**, 152114 (2013).

[19] J. G. Reynolds and C. L. Reynolds, Progress in ZnO acceptor doping: What is the best strategy? Adv. Condens. Matter Phys. **2014**, 457058 (2014).

[20] G. Petretto and F. Bruneval, Comprehensive *Ab Initio* Study of Doping in Bulk ZnO with Group-V Elements, Phys. Rev. Appl. **1**, 024005 (2014).

[21] N. H. Nickel and M. A. Gluba, Defects in Compound Semiconductors Caused by Molecular Nitrogen, Phys. Rev. Lett. **103**, 145501 (2009).

[22] J. M. Philipps, J. E. Stehr, I. Buyanova, M. C. Tarun, M. D. McCluskey, B. K. Meyer, and D. M. Hofmann, Recharging behavior of nitrogen-centers in ZnO, J. Appl. Phys. **116**, 063701 (2014).

[23] J. Heyd, G. E. Scuseria, and M. Ernzerhof, Hybrid functionals based on a screened Coulomb potential, J. Chem. Phys. **118**, 8207 (2003); Erratum: Hybrid functionals based on a screened Coulomb potential [J. Chem. Phys. **118**, 8207 (2003)], *ibid.* **124**, 219906 (2006).

[24] https://www.vasp.at/.

[25] G. Kresse and J. Furthmiiller, Efficiency of ab-initio total energy calculations for metals and semiconductors using a plane-wave basis set, Comput. Mater. Sci. **6**, 15 (1996).

[26] G. Kresse and J. Hafner, Norm-conserving and ultrasoft pseudopotentials for first-row and transition elements, J. Phys.: Condens. Matter **6**, 8245 (1994).

[27] G. Kresse and D. Joubert, From ultrasoft pseudopotentials to the projector augmented-wave method, Phys. Rev. B **59**, 1758 (1999).

[28] P. E. Blöchl, Projector augmented-wave method, Phys. Rev. B **50**, 17953 (1994).

[29] P. Giannozzi, S. Baroni, N. Bonini, M. Calandra, R. Car, C. Cavazzoni, D. Ceresoli, G. L. Chiarotti, M. Cococcioni, I. Dabo, A. Dal Corso, S. de Gironcoli, S. Fabris, G. Fratesi, R. Gebauer, U. Gerstmann, C. Gougoussis, A. Kokalj, M. Lazzeri, L. Martin-Samos *et al.*, QUANTUM ESPRESSO: a modular and open-source software project for quantum simulations of materials, J. Phys.: Condens. Matter **21**, 395502 (2009).

[30] J. P. Perdew, K. Burke, and M. Ernzerhof, Generalized Gradient Approximation Made Simple, Phys. Rev. Lett. **77**, 3865 (1996).

[31] P. Mori-Sánchez, A. J. Cohen, and W. Yang, Many-electron self-interaction error in approximate density functionals, J. Chem. Phys. **125**, 201102 (2006).

[32] M. Cococcioni and S. de Gironcoli, Linear response approach to the calculation of the effective interaction parameters in the LDA + U method, Phys. Rev. B **71**, 035105 (2005).

[33] I. Dabo, A. Ferretti, N. Poilvert, Y. Li, N. Marzari, and M. Cococcioni, Koopmans' condition for density-functional theory, Phys. Rev. B **82**, 115121 (2010).

[34] S. Lany and A. Zunger, Generalized Koopmans density functional calculations reveal the deep acceptor state of N$_O$ in ZnO, Phys. Rev. B **81**, 205209 (2010).

[35] A. Boonchun, W. R. Lambrecht, J. T-Thienprasert, and S. Limpijumnong, Nitrogen pair- hydrogen complexes in ZnO and p-type doping, MRS Online Proc. Libr. **1394**, 27 (2012).

[36] F. Oba, M. Choi, A. Togo, and I. Tanaka, Point defects in ZnO: an approach from first principles, Sci. Tech. Adv. Mater. **12**, 034302 (2011).

[37] J. Bang, Y.-Y. Sun, D. West, B. K. Meyer, and S. Zhang, Molecular doping of ZnO by ammonia: a possible shallow acceptor, J. Mater. Chem. C **3**, 339 (2015).

[38] See Supplemental Material at http://link.aps.org/supplemental/10.1103/PhysRevMaterials.6.104609 for tests on Koopmans's theorem, structural details, and transition levels, which includes Ref. [55].

[39] C. Freysoldt, B. Grabowski, T. Hickel, J. Neugebauer, G. Kresse, A. Janotti, and C. G. Van de Walle, First-principles calculations for point defects in solids, Rev. Mod. Phys. **86**, 253 (2014).

[40] C. G. Van de Walle and P. E. Blöchl, First-principles calculations of hyperfine parameters, Phys. Rev. B **47**, 4244 (1993).

[41] E. van Lenthe, E. J. Baerends, and J. G. Snijders, Relativistic regular two-component Hamiltonians, J. Chem. Phys. **99**, 4597 (1993).

[42] E. van Lenthe, E. J. Baerends, and J. G. Snijders, Relativistic total energy using regular approximations, J. Chem. Phys. **101**, 9783 (1994).

[43] T. Scholl, R. Holt, and S. Rosner, Fine and hyperfine structure in $^{14}N_2^+$: The $B^2\Sigma_u^+$-$X^2\Sigma_g^+(0,0)$ band, J. Mol. Spectrosc. **192**, 424 (1998).

[44] L. B. Knight, J. M. Bostick, R. W. Woodward, and J. Steadman, An electron bombardment procedure for generating cation and neutral radicals in solid neon matrices at 4 K: ESR study of $^{14}N_2^+$ and $^{15}N_2^+$, J. Chem. Phys. **78**, 6415 (1983).

[45] D. Galland and A. Herve, ESR spectra of the zinc vacancy in ZnO, Phys. Lett. A **33**, 1 (1970).

[46] N. T. Son, J. Isoya, I. G. Ivanov, T. Ohshima, and E. Janzén, Magnetic resonance identification of hydrogen at a zinc vacancy in ZnO, J. Phys.: Condens. Matter **25**, 335804 (2013).

[47] Y. K. Frodason, K. M. Johansen, T. S. Bjørheim, B. G. Svensson, and A. Alkauskas, Zn vacancy as a polaronic hole trap in ZnO, Phys. Rev. B **95**, 094105 (2017).

[48] Y. K. Frodason, K. M. Johansen, T. S. Bjørheim, B. G. Svensson, and A. Alkauskas, Zn vacancy-donor impurity complexes in ZnO, Phys. Rev. B **97**, 104109 (2018).

[49] A. F. Kohan, G. Ceder, D. Morgan, and Chris G. Van de Walle, First-principles study of native point defects in ZnO, Phys. Rev. B **61**, 15019 (2000).

[50] P. Erhart, K. Albe, and A. Klein, First-principles study of intrinsic point defects in ZnO: Role of band structure, volume relaxation, and finite-size effects, Phys. Rev. B **73**, 205203 (2006).

[51] J. L. Lyons, A. Janotti, and C. G. Van de Walle, Why nitrogen cannot lead to p-type conductivity in ZnO, Appl. Phys. Lett. **95**, 252105 (2009).

[52] C. H. Park, S. B. Zhang, and S.-H. Wei, Origin of p-type doping difficulty in ZnO: The impurity perspective, Phys. Rev. B **66**, 073202 (2002).

[53] S. Falletta, J. Wiktor, and A. Pasquarello, Finite-size corrections of defect energy levels involving ionic polarization, Phys. Rev. B **102**, 041115(R) (2020).

[54] W. R. L. Lambrecht, A. V. Rodina, S. Limpijumnong, B. Segall, and B. K. Meyer, Valence-band ordering and magneto-optic exciton fine structure in ZnO, Phys. Rev. B **65**, 075207 (2002).

[55] C. Freysoldt, J. Neugebauer, and C. G. Van de Walle, Electrostatic interactions between charged defects in supercells, Phys. Status Solidi B **248**, 1067 (2011).